Nuclear Instruments and Methods in Physics Research B 100 (1995) 165–175

ELSEVIER

NIM B
Beam Interactions with Materials & Atoms

An ion beam apparatus for collinear photodetachment experiments

Dag Hanstorp

Department of Physics, Chalmers University of Technology and Göteborg University, S-412 96 Göteborg, Sweden

Received 22 July 1994; revised form received 1 December 1994

Abstract

A new collinear laser–ion beams apparatus, designed for laser photodetachment experiments, is described. The apparatus differs mainly in four aspects from other similar facilities. First, the angular distribution of the electrons emitted in the photodetachment process can be measured although the laser and ion beams are collinearly aligned. This gives an increase of the signal with more than two orders of magnitude in comparison with the conventional crossed beams experiments. Second, a new type of secondary electron emission detector is used to detect neutral atoms produced in the photodetachment process. The detector is capable of preventing the detection of electrons produced by the photoelectric effect induced by the laser radiation; therefore, pulsed lasers, with their high photon fluxes, can be used in experiments with the apparatus. Third, a simplified design of an electrostatic quadrupole deflector, used to bend the ion beam into the laser beam, has been implemented in the apparatus. Finally, a surface ionizer, giving a very low energy spread of the ions, is used to produce the negative ions. A detailed description of the apparatus is given, and examples of measurements of total and differential cross sections and an example of a mass spectrum are presented in the paper.

1. Introduction

The interaction between laser radiation and fast ion beams has been exploited extensively during the last two decades. Initially, the experiments were performed using laser and ion beams interacting at perpendicular angles, but in 1976 a new technique with parallel beams was introduced. Although the crossed beam geometry is still the most frequently used, there are several experiments where the collinear geometry is favorable. The first two experiments with coaxial laser and ion beams were performed by Wing et al. [1] and Dufay et al. [2]. Wing et al. studied HD^+ with a technique whereby a laser beam intercepted an ion beam at a very small angle (≈ 11 mrad). Dufay et al. were the first to utilize completely parallel ion and laser beams in an experiment where they studied Ba^+. Today, the method of collinear laser and fast particle beams has been used for studies of both positive and negative ions as well as for studies of fast beams of neutral atoms.

There are essentially three reasons for using the slightly more complicated method with collinear beams. First, the interaction path increases with two to three orders of magnitude, which, of course, can be essential when weak processes are studied. Secondly, the collinear geometry gives the highest resolution. This is caused by the so called velocity compression which reduces the Doppler broadening, as first pointed out by Kaufman in 1976 [3] (this effect is discussed in Section 3.1). Finally, the laser frequency felt by the ions can easily be tuned by changing the velocity of the ions.

In negative ion spectroscopy, the increased interaction path is of special value since the cross section for the photodetachment process normally is small. This is especially true when the photodetachment threshold, where the cross section goes to zero, is studied. Further, the high optical resolution reached in the collinear geometry is essential in order to get the desired accuracy in many electron affinity determinations.

To the author's knowledge, there are five ion beam apparatuses which have been used for coaxial beam photodetachment experiments on negative ions. The apparatus at *JILA* (Colorado) has been used to determine electron affinities of both atomic and molecular systems [4]. At *SRI International* (California), many metastable states of negative ions as well as molecular negative ions have been investigated [5], and at *University of Oregon*, an apparatus used for infrared spectroscopy has been built [6]. In recent years, two new facilities have been constructed. At *University of Virginia* the photodetachment process in a microwave field has been investigated [7], and in Israel an apparatus for collinear photodetachment combined with a tandem accelerator has been built [8] in which isotope measurements are performed.

* Corresponding author. Tel. +46 317723274, fax +46 317723496, e-mail f3adag@fy.chalmers.se.

SSDI 0168-583X(94)00656-3

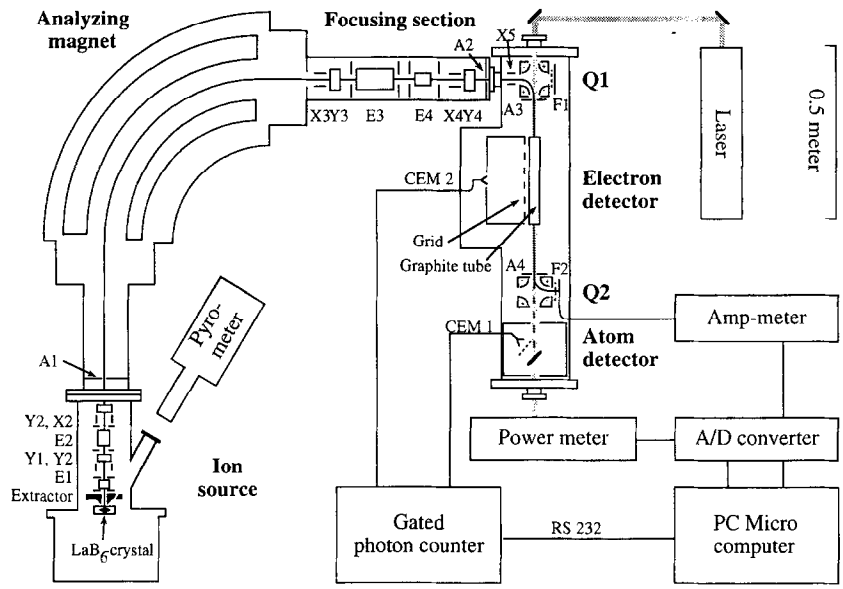

Fig. 1. A schematic diagram of the apparatus.

In this paper a new collinear laser–ion beams apparatus is presented. Its main features are the following:

1) The angular distribution of the electrons emitted in the photodetachment can be measured, although the laser and ion beams are collinearly aligned. The signal then becomes considerably larger than in a crossed beams experiment.

2) A secondary electron emission detector is used to detect neutral atoms produced in the photodetachment process. Normally, such detectors cannot be used in collinear experiments where pulsed laser are used since the laser light then strikes the detector target where it produces an enormous amount of electrons by the photoelectric effect. The detector installed in this apparatus is capable of preventing the detection of these electrons, and pulsed lasers can therefore be used.

3) A new simplified type of a electrostatic quadrupole beam deflector, used to merge the ion beam with the laser beam, has been designed and implemented in the apparatus.

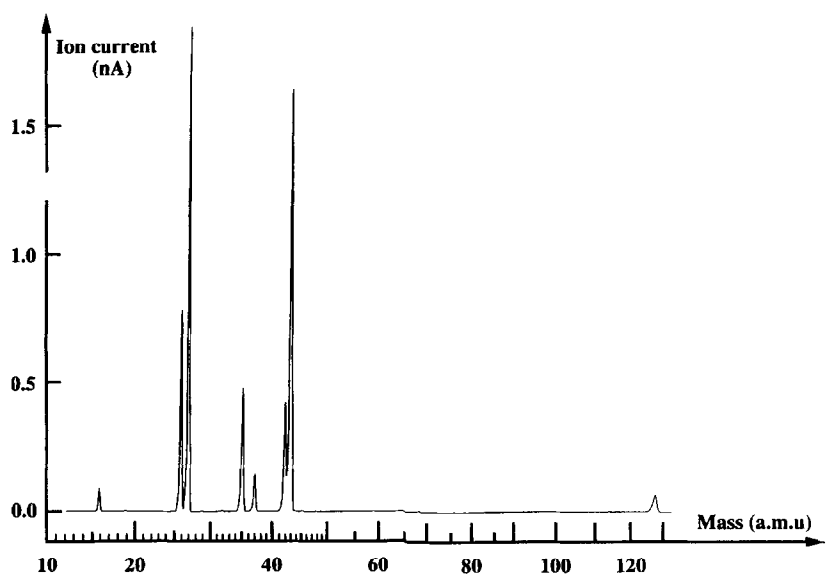

Fig. 2. Background mass spectra from the LaB_6 ionizer. The main components in the spectrum are O^- ($m = 16$), BO^- ($m = 26$ and 27), CN^- ($m = 26$), Cl^- ($m = 35$ and 37), BO_2^- ($m = 42$ and 43) and I^- ($m = 127$).

4) It is equipped with an ion source which produces ions with a small energy spread. The source can primarily be used to produce negative ions with relatively large electron affinities.

2. Description of the apparatus

2.1. Overview

In this section a detailed description of the apparatus is given. A schematic diagram of the apparatus is shown in Fig. 1. Basically, negative ions are formed in an ion source, mass analyzed with a sector magnet and directed into an analyzing chamber where they are merged with a laser beam. A negative ion which absorbs a photon is divided into a neutral atom and a free electron, both of which can be detected.

2.2. Ion source

A negative surface ionizer (NSI) is used to produce the ions. The ionizer is made of LaB_6-powder which is pressed onto a tantalum rod. LaB_6 was chosen due to its low work function (2.7 eV). The rod, with a diameter of 3 mm, is resistively heated with a direct current of approximately 100 A. When heated, the LaB_6-powder forms a crystal which can ionize atoms and molecules adsorbed on its surface. There is a strong emission of electrons from the crystal which is several orders of magnitude larger than the ion current. A weak magnetic field from an electromagnet is applied over the ion source in order to deflect these electrons out of the beam.

The ion source produces a number of ions originating from the interior of the crystal which, besides lanthanum and boron, contains traces of several other elements. These other elements diffuse towards the surface where they are ionized. Fig. 2 shows a mass spectrum recorded with an ionizer temperature of 1200°C and an ion source pressure of 1×10^{-5} mbar obtained by leaking air into the vacuum chamber.

In order to produce a specific ion, a suitable gas is leaked into the ion source. For instance, inlet of halogen dimers (e.g. I_2) gives ion currents of atomic halogen negative ions of the order of 1 μA, stable over several days. Ion currents of other elements can be produced if the electron affinity is larger than 1.5 eV, but the ion current is usually much smaller and more unstable. In general, experiments have shown that the surface of the ionizer very easily becomes contaminated, making the choice of gas critical.

2.3. Ion optics

In the analyzing chamber, the negative ions interact with laser light in a region defined by two round holes, with a diameter of 3 mm and placed 50 cm apart, giving a beam divergence of 6 mrad (half angle). A high transmission of ions through these two holes was the primary criteria when designing the ion optics. A computer simulation program [9] was used to simulate the beam paths; the program first calculated the electrical field for a given geometry, and subsequently a ray tracing routine was executed where the ion beam trajectories were calculated.

As mentioned in Section 2.2, the ions are formed on a LaB_6-crystal pressed onto a tantalum rod, where the area of the crystal is approximately 1 mm^2. The cross section of the ion beam depends on the size of the crystal; a small crystal is necessary in order to produce a well collimated ion beam. On the other hand, a smaller crystal has to be

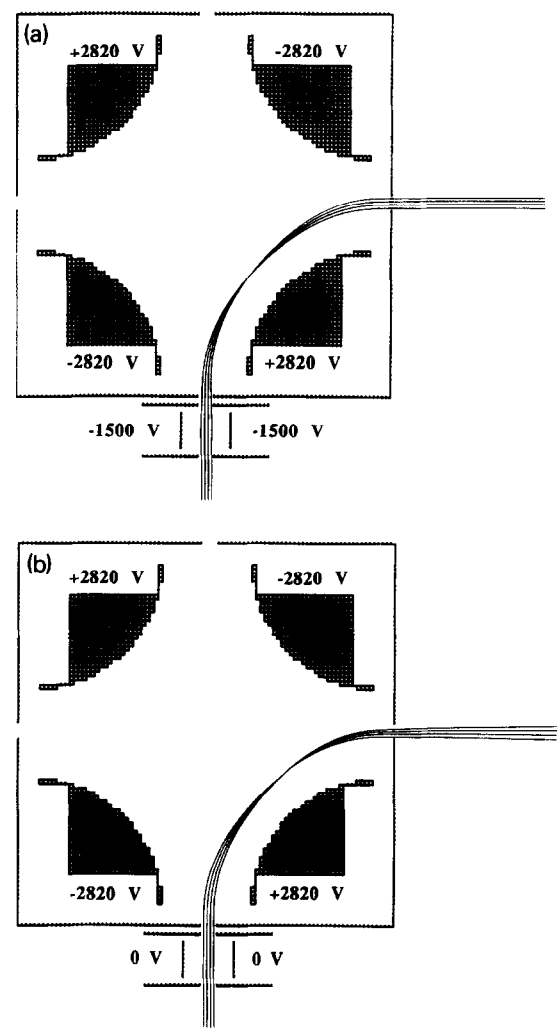

Fig. 3. A computer simulation of ion beam paths in the electrostatic quadrupole beam deflectors. The ions, which have an energy of 3000 eV, enter the quadrupole from below; (a) and (b) differ only in the potential of the deflection plates (X5 in Fig. 1) in front of the quadrupole.

hotter in order to produce the same ion current, and this increases the evaporation of the crystal and hence shortens its lifetime.

The ions are accelerated with an electric field applied between the ionizing surface, at negative potential, and the extractor, at ground potential. The acceleration voltage is typically 3 kV. A 2 mm diameter hole in the extractor direct the ions into a system consisting of two Einzel lenses (E1, E2) and four pairs of deflection plates (X1, Y1, X2, Y2). After the second Einzel lens, the ions are sent through a 90°-sector magnet with a radius of 0.5 m. The magnet is capable of bending all atomic ions with energies of 5 keV. Two Einzel lenses (E3, E4) and four pairs of deflection plates (X3, Y3, X4, Y4) are placed in the focusing section after the magnet. They are used to steer and focus the ion beam onto a small aperture (A2) leading into the analyzing chamber.

In the analyzing chamber the ions are deflected 90° into the laser beam. After a 50 cm long drift region, the ions are bent 90° a second time where a Faraday cup (F2) measures the ion current. The ions are deflected by means of two electrostatic quadrupole deflectors (Q1, Q2) whose axes are perpendicular to the laser and ion beams. The quadrupole beam deflector was originally designed by Zeman [10], but the deflectors used in this apparatus have been simplified in their mechanical construction. The shim electrodes, which are used to compensate for the fringe fields at the entrance and exit of the quadrupole, have been replaced by a pair of deflection plates (X5) placed in front of the quadrupole. The deflection plates, working in the horizontal plane, compensate for the small focusing property of the quadrupole deflector (Fig. 3).

The mass resolution of the apparatus has been determined to be $M/\Delta M = 80$ when the apparatus has been optimized for maximum transmission. This value can be increased, by adjusting the beam parameters, to $M/\Delta M = 170$, but at the cost of a less intense ion beam.

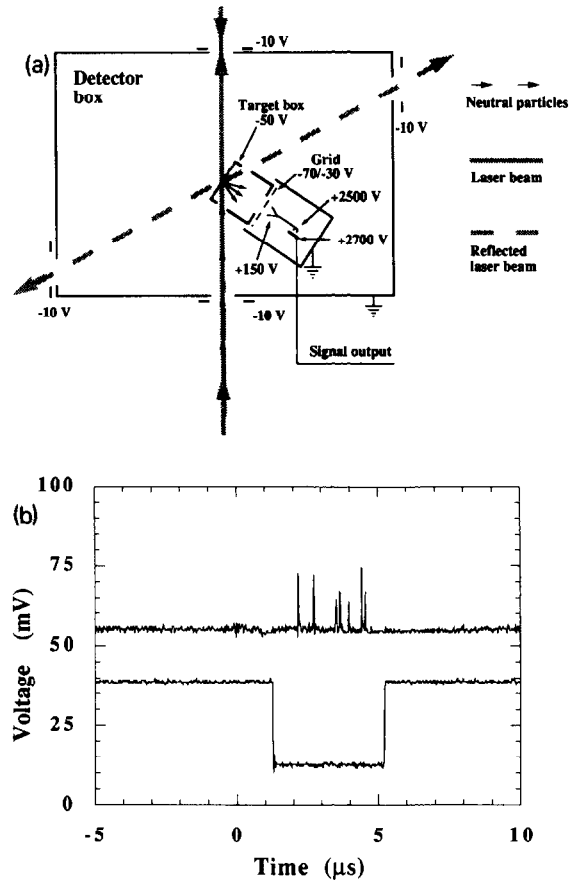

Fig. 4. (a) A schematic figure of the neutral atom detector. (b) Oscilloscope trace of the output from the channel electron multiplier (upper curve) and the enabling time of the photon counter (lower curve). The laser is triggered at $t = 0.0$ μs and the detector is opened by switching the potential on the grid in front of the CEM at $t = 1.0$ μs.

2.4. Detectors

i) Ion current detectors

The ions pass several apertures (A1–A4) along the beam path, where each aperture is separately connected to an ampèremeter. A Faraday cup, which is used to measure the absolute ion current, is placed on each quadrupole (F1, F2). The Faraday cup is simply a metal plate connected to an ampèremeter. A fine mesh, biased to −20 V, is mounted in front of the plate. The ions can penetrate the mesh, but secondary electrons emitted from the metal plate are repelled.

ii) Neutral particle detector

Neutral atoms produced in the photodetachment process in the region between the two quadrupoles are not affected by the second quadrupole (Q2); instead they traverse to a neutral atom detector placed behind Q2. The detector, shown in Fig. 4a, has been described in detail elsewhere [11] and only its main features are presented here. The atoms impinge on a glass plate where secondary electrons are produced which are detected with a Channel Electron Multiplier (CEM1). A thin layer of In_2O_3:Sn on the surface of the glass plate prevents it from being charged. A grid is placed between the glass plate and the entrance cone of the CEM. The voltage on the grid can be biased so it either permits or prevents electrons produced in the glass plate to reach the CEM. This feature is used to solve a serious problem introduced if pulsed laser light is used: The intense radiation produces an enormous amount of electrons in the glass plate by the photoelectric effect. The signal can be so intense that it strongly saturates the CEM, resulting in a recovery time of tens of microseconds. Fortunately, the laser pulse arrives at the glass plate some

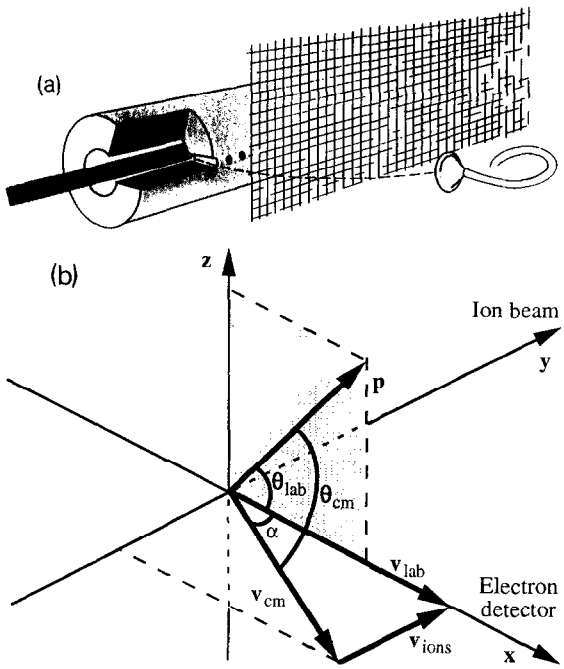

Fig. 5. (a) The electron detector with angular resolution. The dark line in the centre of the tube represents the ion and laser beams while the dashed line represents the trajectory of a detected electron. (b) The geometry of the electron detector. The notation is explained in Section 5.3.

time before the neutral particles, due to the travelling time of the atoms from the region between the quadrupoles to the glass plate. It is then possible to block the CEM during the laser pulse, with a duration of typically 20 ns, and then open it before the first neutral atoms arrive about 1 μs after the laser pulse. A timing diagram for the detector is shown in Fig. 4b.

iii) Electron detector with angular resolution

A new detector, shown in Fig. 5a, which is used to measure the angular distribution of the emitted electrons, has been developed. In contrast to previous detectors with angular resolution, the ion and laser beams are here collinearly aligned. This gives a signal which is more than two orders of magnitude larger than the signal achieved with perpendicular laser and ion beams. A first experiment with the detector has been described in Ref. [12].

The detector is made from a 250 mm long graphite tube, with an outer diameter of 32 mm and an inner diameter of 13 mm, which is placed with its central axis on the beam path. Graphite was chosen due to its stability against contact potential changes (small patch fields). The tube has 67 holes with a diameter of 2.5 mm drilled along one side, and a grounded stainless steel mesh is placed outside the holes. A channel electron multiplier (CEM2) is placed 10 cm behind the mesh facing the holes in the graphite tube. Electrons passing any of the holes are attracted by CEM2 by a positive potential on its front cone. Only electrons emitted perpendicularly with respect to the ion and laser beams are transmitted through the holes and can reach the CEM. Electrons emitted in any other direction hit the inner wall of the tube where they are grounded. The angular distribution is measured by rotating the polarization of the laser light. The detector is placed inside a double layer μ-metal box in order to reduce the magnetic field.

2.5. Data acquisition

The two CEMs used in the apparatus are both run in a pulse counting mode in which each detected particle gives rise to a 15 ns long pulse. The pulses are amplified with fast pre-amplifiers and fed into a photon counter with two independent counters. The two counters can either be used to count the signal from the two CEMs, or they can be used to measure the signal and the background from one of them.

The entire experiment is controlled by a PC micro computer which is interfaced with the photon counter via an IEEE interface. An A/D-converter is used to register the signal from an amperemeter, used to measure the ion current, and the signal form a laser power meter.

2.6. Vacuum system

The vacuum system, finally, is divided into three separate sections: the ion source, the focusing section, which includes the analyzing magnet, and the analyzing chamber. The first two chambers are constructed for high vacuum, while the third section is designed with ultra high vacuum (UHV) technology.

The vacuum chambers for the ion source and for the focusing section are pumped with diffusion pumps with liquid nitrogen baffles. The base pressure in these two chambers is 10^{-7} mbar, but the pressure in the ion source during operation is usually considerably higher due to the inlet of different gases. The opening between the ion source and the focusing section is limited to a small aperture (A1). This diminishes leakage from the ion source into the focusing section.

The UHV-system in the analyzing chamber is a completely oil-free system with a base pressure of less than 10^{-9} mbar. A membrane pump and two sorption pumps are used for roughing, while the main pump is an ion pump. Leakage through the small aperture (A2) separating the focusing and the analyzing chambers is the main contributor of residual gas in the analyzing chamber. Since this is the entrance for the ion beam, decreasing the size of the hole also decreases the ion current.

3. Performance of the apparatus: General considerations

3.1. Optical resolution

i) The Doppler shift

One of the most striking effects with the collinear geometry is the large Doppler shift. If the absolute wavelength felt by the ions is of interest, the measured wavelength has to be corrected for this effect. In experiments performed with low optical resolution, the unshifted wavenumber can simply be calculated with the non-relativistic Doppler formula,

$$\sigma^{\mathrm{p,a}} = \sigma_0\left(1 \pm \frac{v}{c}\right), \tag{1}$$

where σ_0 is the unshifted wavenumber, $\sigma^{\mathrm{p,a}}$ is the measured wavenumber, v is the ion velocity and p and a indicate whether the ion and laser beams are parallel or antiparallel. An ion velocity of 10^5 m/s and a wavelength of 500 nm gives, according to Eq. (1), a non-relativistic Doppler shift of 6.7 $\mathrm{cm}^{-1} \approx 200$ GHz.

If the experiment is performed with high resolution, the velocity of the ions has to be determined with a more accurate method. This can be done by performing two independent measurements, in which the laser and ion beams are parallel and antiparallel respectively. The Doppler shift now has to be calculated using the relativistic Doppler formula

$$\sigma^{\mathrm{p,a}} = \frac{\sigma_0\left(1 \pm \frac{v}{c}\right)}{\sqrt{1-\left(\frac{v}{c}\right)^2}}. \tag{2}$$

By taking the geometrical mean of the two measured quantities, the Doppler effect is eliminated to all orders in (v/c) and the unshifted wavenumber can be determined:

$$\sqrt{\sigma^{\mathrm{p}}\sigma^{\mathrm{a}}} = \sqrt{\frac{\sigma^0\left(1+\frac{v}{c}\right)}{\sqrt{1-\left(\frac{v}{c}\right)^2}}\,\frac{\sigma_0\left(1-\frac{v}{c}\right)}{\sqrt{1-\left(\frac{v}{c}\right)^2}}} = \sqrt{\sigma_0\sigma_0} = \sigma_0. \tag{3}$$

ii) Energy spread of the ions

Doppler broadening is usually a serious problem in high resolution spectroscopy, but by using the collinear geometry it can be decreased considerably. The initial energy spread of the ions, due to the non-zero temperature in the ion source, is compressed if all ions are accelerated over the same electrical potential [3]. The compressed velocity spread is obtained by differentiating the expression for the kinetic energy:

$$\Delta v = \frac{\Delta W}{\sqrt{2mW}}. \tag{4}$$

The velocity spread of ions emitted from a LaB_6 ionizer has been determined by Kashihira et al. [13] to be 0.55 eV. As an example, Eq. (4) gives a residual velocity spread of 15 m/s for chlorine ions accelerated to 2 keV. This corresponds to a frequency width of 30 MHz if the wavelength of the laser light is 500 nm.

iii) The divergence of the ion and laser beams

In general, the frequency uncertainty caused by the divergence of the laser and ion beams can be determined to

$$\Delta\nu = \nu_0\left(1-\frac{v}{c}\cos(\theta+\Delta\theta)\right) - \nu_0\left(1-\frac{v}{c}\cos\theta\right), \tag{5}$$

where θ is the angle between the laser and ion beams. In a collinear geometry, when $\theta = 0$, this becomes

$$\Delta\nu = \nu_0\frac{v}{c}(-\cos\Delta\theta+1) \approx \nu_0\frac{v}{c}\left(-1+\frac{(\Delta\theta)^2}{2}+1\right) = \frac{v}{\lambda_0}\frac{(\Delta\theta)^2}{2}. \tag{6}$$

The divergence of the ion beam, which has a half angle of 6 mrad, is given by the diameter and separation of the defining apertures in the interaction region. The divergence of the laser beam can easily be made substantially smaller, resulting in a total laser–ion beam divergence of 6 mrad. This corresponds to a frequency width of 4 MHz for an ion beam velocity of 10^5 m/s and a wavelength of 500 nm.

iv) The interaction time

The frequency uncertainty due to the finite interaction time is given by Heisenberg's uncertainty relation:

$$\Delta E\,\Delta t \geq \hbar/2,$$

$$h\,\Delta\nu\,\Delta t \geq (h/2\pi)/2,$$

$$\Delta\nu \geq 1/(4\pi\,\Delta t) \approx 1/(10\Delta t) \tag{7}$$

The interaction time, i.e. the time which an ion is illuminated by the laser radiation, depends on whether a pulsed or a cw (continuous wave) laser is used. With a cw laser, the time is determined by the transit time for the ions between the two quadrupoles. A typical value of the transit time is 5 μs, which gives a frequency uncertainty of only 16 kHz. If pulsed lasers are used, the interaction time is given by the pulse length of the laser radiation, where a pulse length of 20 ns gives a frequency uncertainty of 4 MHz.

v) Frequency widths of lasers

The design of the apparatus allows both cw and pulsed lasers to be used to study the photodetachment process. There are commercially available dye cw lasers with frequency widths of 1 MHz, while the best pulsed lasers have bandwidths on the order of 1 GHz. Although the frequency widths of the two laser types differ by three orders of magnitude, the resolutions achieved in actual experiments differ considerably less. The best resolution achieved using a cw laser is 180 MHz in an experiment where the electron affinity of oxygen was determined [4,14]. With pulsed lasers, the highest resolution so far has been achieved with the apparatus described in this paper in an experiment where the electron affinity of iodine was determined with an accuracy of 2.4 GHz [15]. The reason for not reaching the resolution which could be expected with cw lasers is the relatively large statistical uncertainty in the experiments. In the next section it is shown that the signal to noise ratio is typically three orders of magnitude better when pulsed, instead of cw, lasers are used.

vi) Total frequency width

If narrow band cw lasers are used in the experiments the total frequency width is determined by the properties of the apparatus. The frequency width due the velocity spread of the ions then dominates, giving a frequency width around 30 MHz. The bandwidth of the laser of 1 MHz is then negligible. With a pulsed laser, on the other hand, the effective bandwidth in an experiment is entirely determined by the bandwidth of the laser.

3.2. Signal considerations

i) Cw lasers

The intensity of the radiation from a typical cw dye laser focussed in the interaction region of the apparatus is around 2 W/cm^2. The probability for photodetachment, p_γ, can then be estimated to be

$$p_\gamma = \frac{I_\gamma \sigma_\gamma L}{v E_\gamma} = \frac{2\,\mathrm{W/cm^2} \times 10^{-18}\,\mathrm{cm^2} \times 50\,\mathrm{cm}}{10^7\,\mathrm{cm/s} \times 4 \times 10^{-19}\,\mathrm{W\,s}} = 2.5 \times 10^{-5}. \quad (8)$$

where I_γ is the laser intensity, σ_γ the photodetachment cross section, L the interaction length, v the ion beam velocity and E_γ, finally, the photon energy. Similarly, the probability for collisional detachment, p_c, is estimated to

$$p_c = \sigma_c n L = 10^{-15}\,\mathrm{cm^2} \times 4 \times 10^7/\mathrm{cm^3} \times 50\,\mathrm{cm} = 2.0 \times 10^{-6}, \quad (9)$$

where n is the density of particles in the background gas ($p = 10^{-9}$ mbar). This gives a signal which is one order of magnitude larger than the background. With an ion current of 0.1 nA, an ion current obtainable for many negative ions, one gets 10^4 photodetached and 10^3 collisionally detached negative ions per second.

The same signal to background ratio is obtained with the angular distribution electron detector but the count rates are much smaller. The collection efficiency has been estimated to 10^{-3} assuming an isotropic emission of the electrons. With the same ion current one would get 10 photodetached and 1 collisionally detached electrons per second.

ii) Pulsed lasers

The signal level increases drastically if pulsed, instead of cw, lasers are used. The interaction time is now determined by the laser pulse duration Δt, which for an excimer pulsed dye laser is about 20 ns. During this time the negative ions only move a few millimeters, while the interaction region is 500 mm long. Therefore, the laser light only interacts with ions which already are in the interaction region when the laser is triggered. The probability for photodetachment can now be estimated to be

$$p_\gamma = \frac{I_\gamma \sigma_\gamma \Delta t}{E_\gamma} = \frac{10^6\,\mathrm{W/cm^2} \times 10^{-18}\,\mathrm{cm^2} \times 20\,\mathrm{ns}}{4 \times 10^{-19}\,\mathrm{W\,s}} = 0.05. \quad (10)$$

The probability for collisional detachment is, of course, independent of the type of laser used in the experiment. The signal to background ratio then becomes 25 000, an improvement with more than three orders of magnitude in comparison with cw laser experiments. Correspondingly, the signal to background ratio from the angular distribution electron detector will be enhanced with the same ratio.

The extremely good signal to background ratio obtained when pulsed lasers are used cannot always be fully used since the CEM very easily will be saturated. The signal from one laser pulse arrives at the detector within a few microseconds. Each pulse is approximately 15 ns long, but the maximum count rate is around 10 MHz, allowing a maximum of around 50 neutral particles to be detected per laser pulse. With the angular distribution detector this problem is even more pronounced. In this case all electrons produced by one laser pulse arrive at the CEM within 50 ns. This means that only one electron per laser pulse can be detected.

4. Total cross section measurements

4.1. Absolute total cross sections

The total cross section can be determined through the relation

$$\sigma_\gamma = \frac{(\text{number of photodetached ions})}{\Delta t(\text{number of ions})(\text{number of photons})} = \frac{(N_\gamma/\eta)}{\Delta t(I_{\mathrm{ion}}/q)(I_\gamma/E_\gamma)} = \frac{N_\gamma q E_\gamma}{\Delta t\,\eta I_{\mathrm{ion}} I_\gamma}, \quad (11)$$

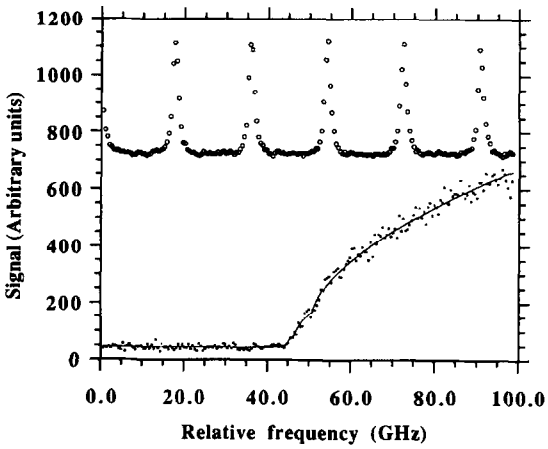

Fig. 6. Relative photodetachment cross section of iodine. The increase represents the onset of the transition from the ground state of I^- to the ground state of I. The solid line is a fit to the Wigner law superimposed on a linear background. The small humps in the figure are due to the hyperfine structure in the ground state of I^-. The upper points (open circles) are the recording of a Fabry–Perot reference spectrum.

where N_γ is the count rate of the detected neutral particles, η the detection efficiency of the neutral atom detector, Δt the interaction time, I_{ion} is the ion current and q the elementary charge. When cw lasers are used, Δt is the transit time for the ions through the interaction region, while for pulsed lasers it is determined by the laser pulse length. In order to make an absolute determination of total photodetachment cross section, all quantities in Eq. (11) have to be measured absolutely. Some of these quantities, such as the interaction time, can easily be determined with reasonable accuracy, while others, like the detection efficiency η of the neutral particle detector suffer from a large uncertainty. Furthermore, a determination of the cross section requires a uniform distribution of the ion and laser beams in the interaction region, which is not necessarily true. In order to perform such an experiment, the spatial distribution of both the ion and laser beams need to be investigated.

4.2. Relative total cross sections

Relative cross sections can, on the other hand, be measured with high accuracy, and the result shown in Fig. 6 may serve as an example of this. The figure shows the relative photodetachment cross section of iodine as a function of the laser wavelength. The dots are the data points, with a step size of 0.5 GHz, and the solid line is a least squares fit to the Wigner law [16]. There are four independent photodetachment channels, each corresponding to different hyperfine structure components in the final state, i.e. the neutral iodine atom. The bandwidth of the laser is 1.2 GHz, and the difference between the hyperfine structure components are 0.74, 1.97 and 4.23 GHz respectively. The number of photodetached negative ions has been normalized both with respect to the ion current, measured after the second quadrupole, and with respect to the intensity of the laser light, measured after the vacuum chamber. The scattering in the data corresponds to the shot noise ($\chi^2 = 0.99$), which indicates that the normalization procedure works efficiently.

The method to measure relative total photodetachment cross sections can easily be used to compare the result from different negative ions by switching the mass separator between the two masses of interest. In this way the photodetachment cross sections for any negative ion can be compared with well known cross sections.

5. Differential cross section measurements

5.1. Angular distribution: definitions

In the electric dipole approximation, the differential cross section for emission of photo-electrons is given by the formula

$$\frac{d\sigma}{d\Omega} = \frac{\sigma}{4\pi}\left[1 + \beta P_2(\cos\theta)\right], \tag{12}$$

where σ is the total cross section described in the previous section, β the asymmetry parameter and $P_2(\cos\theta)$ is the Legendre polynomial of second order which can be written as

$$P_2(\cos\theta) = \frac{3\cos^2\theta - 1}{2}. \tag{13}$$

θ is the angle between the emitted electron and the polarization vector of the laser light. The ions are assumed to be unpolarized while the laser light is assumed to be linearly polarized. The formula shows that, within the given assumptions, it is only the asymmetry parameter that determines the angular distribution. Consequently, β can be determined if the electron yield is known for two independent directions. β can vary between -1, where the electron distribution has a pure $\sin^2\theta$ behaviour, via β equals zero, where the distribution is isotropic, to β equals 2 where the distribution has a pure $\cos^2\theta$ behaviour.

5.2. An example of a differential cross section measurement

The angular distribution of electrons emitted in the photodetachment process from O^-, using the 488 nm line in an Ar^+-laser, is shown in Fig. 7. The angle θ_{lab} is defined as the angle between the direction of electron collection and the polarization vector of the light (in the laboratory frame). The electron yield in one specific direction is measured, and the angular distribution is obtained

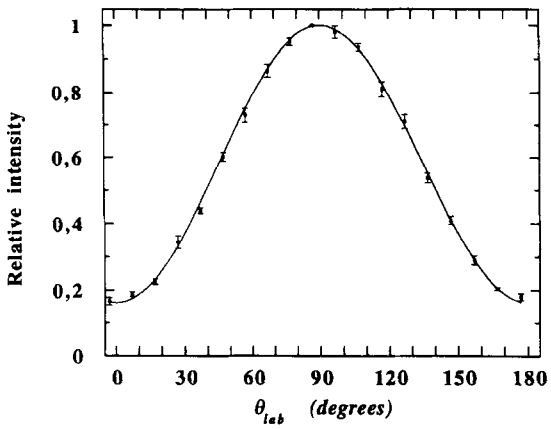

Fig. 7. Angular distribution of electrons photodetached from O^- at 488 nm. The points are the measured values and the solid line is a least squares fit of the measured values.

by rotating the laser polarization by means of a linear polarizer in combination with a $\lambda/2$ plate. The result is normalized with respect to the signal from the neutral particle detector. This compensates for fluctuations in both the ion and laser beam intensities, as well as changes in the overlap between the two beams. The intensity at $\theta_{lab} = 90°$ is set to 1.

5.3. Determination of the asymmetry parameter β

The measured angular distribution has to be corrected for two effects before a correct value of the asymmetry parameter can be deduced.

The *kinematic effect* is caused by the fact that the experiment is performed in the lab frame while the physically interesting information is contained in the centre-of-mass frame. A correction of the kinematic effect is therefore equal to a transformation from the lab to the centre-of-mass frame. Fig. 5b shows the geometry of the experiment, where the ion and laser beams are directed along the y-axis and the detector collects electrons emitted along the x-axis. Electrons directed along the x-axis in the lab frame with the velocity v_{lab} have been ejected slightly backwards in the centre-of-mass frame with the velocity v_{cm}. The angle between the emitted electrons and the laser polarization (p) in the centre-of-mass frame, θ_{cm}, is related to θ_{lab} according to the relation

$$\cos(\theta_{cm}) = \cos(\alpha)\cos(\theta_{lab}), \tag{14}$$

where α is the angle between the direction of the emitted electron in the laboratory and centre-of-mass frames. α can be determined through the relation

$$\sin(\alpha) = \frac{|v_{ions}|}{|v_{cm}|}, \tag{15}$$

where v_{ions} is the velocity of the ions and v_{cm} the velocity of the electrons in the centre-of-mass frame. The velocity of the emitted electrons in the centre-of-mass frame is given by

$$|v_{cm}| = \sqrt{\frac{2(h\nu - E_b)}{m_e}}, \tag{16}$$

where $h\nu$ is the photon energy, E_b the binding energy of the electron and m_e is the electron mass. The recoil energy of the neutral atom and the momentum of the photon have then been neglected.

Eq. (15) shows that the kinematic effect becomes larger when v_{cm} is decreased. If v_{cm} is smaller than v_{ions}, it is not possible to detect any electrons; there is no direction of the vector v_{cm} which corresponds to v_{lab} directed along the x-axis.

A special case occurs if $\theta_{lab} = 90°$, i.e. if the laser polarization is directed along the z-axis. Eq. (14) then gives $\theta_{cm} = 90°$, independently of the value of α. In this case all electrons emitted in the x–y plane are emitted in a direction perpendicular to the laser polarization.

The experiment shown in Fig. 7 is now treated as an example of the kinematic effect. The velocity of the ions, v_{ions}, was 176000 m/s and the velocity of the emitted electrons in the centre-of-mass frame, v_{cm}, was 616000 m/s. The angle α can then, according to Eq. (15), be determined to be 16.6°. The intensity at $\theta_{lab} = 0°$ was determined with a least squares fit to be 0.162 when the intensity at $\theta_{lab} = \theta_{cm} = 90°$ was set to unity. In order to extract the value of the β parameter, we now need to calculate the intensity for $\theta_{cm} = 0°$. From Eqs. (12) and (13) it follows that the angular distribution can be expressed as

$$I_{cm}(\theta_{cm}) = I_{cm}(0°) + [1 - I_{cm}(0°)]\sin^2\theta_{cm}. \tag{17}$$

From Eq. (14) it follows that $\theta_{cm} = \alpha$ when $\theta_{lab} = 0°$, which means that

$$I_{lab}(0°) = I_{cm}(\alpha). \tag{18}$$

Combining Eqs. (17) and (18) one obtains

$$I_{lab}(0°) = I_{cm}(0°) + [1 - I_{cm}(0°)]\sin^2\alpha. \tag{19}$$

Solving for $I_{cm}(0°)$ this becomes

$$I_{cm}(0°) = \frac{I_{lab}(0°) - \sin^2\alpha}{1 - \sin^2\alpha}. \tag{20}$$

With $\alpha = 16.6°$ and $I_{lab}(0°) = 0.162$ we, finally, get $I_{cm}(0°) = 0.087$.

The *non-zero acceptance angle* is the second effect which has to be considered before the asymmetry parameter can be determined. The detector has a fairly large acceptance angle, with $\pm 6°$ in the x–z plane and $\pm 15°$ in the x–y plane, but this has only a small influence on the measured angular distribution. When θ_{lab} equals 90°, all electrons emitted in the x–y plane are perpendicular to the laser polarization making $\theta_{cm} = 90°$ for all detected electrons. The $\pm 6°$ acceptance angle in the x–z plane then has

a negligible effect on the measured value. When $\theta_{lab} = 45°$, the angular distribution function can be approximated with a linear function, and also in this case the non-zero acceptance angle has negligible effect on the results. Therefore, the non-zero acceptance angle affects the result only when $0° \leq \theta_{lab} < 45°$.

The correction for the combined effects of the kinematic effect and the non-zero acceptance angle is performed by integration over all emission angles, and this has been made by means of a computer program. The corrected value of $I_{cm}(0°)$ has then been determined to be 0.078, which differs with 0.009 from the value that had been corrected only for the kinematic effect.

The *asymmetry parameter* β can easily be calculated when $I_{cm}(0°)$ and $I_{cm}(90°)$ are known. With the aid of Eqs. (12) and (13) one obtains

$$\frac{I_{cm}(0°)}{I_{cm}(90°)} = \frac{\frac{\sigma}{4\pi}\left[1 + \beta P_2(\cos 0°)\right]}{\frac{\sigma}{4\pi}\left[1 + \beta P_2(\cos 90°)\right]} = \frac{\left[1 + \beta\left(3\cos^2(0°) - 1\right)/2\right]}{\left[1 + \beta\left(3\cos^2(90°) - 1\right)/2\right]} = \frac{[1 + \beta]}{[1 - \beta/2]}. \tag{21}$$

Solving for β we get

$$\beta = \frac{2\left(\frac{I_{cm}(0°)}{I_{cm}(90°)}\right) - 2}{\left(\frac{I_{cm}(0°)}{I_{cm}(90°)}\right) + 2}. \tag{22}$$

With $I_{cm}(0°) = 0.078$ and $I_{cm}(90°) = 1$, we obtain a β value of -0.887.

5.4. Estimation of systematic errors

In Section 3.2 it was shown that the signal level achieved with the electron detector was very small in comparison with the signal level achieved with the neutral atom detector. Despite this, the electron detector is a very powerful tool; the signal from the electron detector can be normalized in two ways, making the signal less sensitive for fluctuations. First of all the signal can be compared with the signal from the neutral particle detector. Changes in the ion beam and laser beam intensities as well as changes in the overlap influence the signal from the two detectors in the same way. Secondly, the β value is deduced from the ratio of the intensities in two independent directions. β can therefore be determined without measuring the ion current, the laser power or the overlap with absolute methods. Consequently, the measured differential cross section can with reliability be compared with theoretical calculations.

Previously, the influences of the kinematic effect and the non-zero acceptance angle have been discussed. Although both effects change the measured values, they do not increase the error in measurement; both effects can be estimated and the measured value can be corrected. More serious, however, are effects which change the measured value, and which are more difficult, or impossible, to estimate. An upper limit of the errors must be estimated, which should be added to the systematical errors in the experiment.

The *residual magnetic field* has been measured with a gauss meter and found to be less than 10 mG. An 1 eV electron which moves perpendicularly with respect to a magnetic field of 10 mG is moving in a circle with a radius of 3.4 m. The electron path in the field free region is 16 mm long, and the magnetic field can then maximally deflect an electron 40 μm. This deflection is negligible in comparison with the size of the small holes in the graphite tube and the residual magnetic fields does therefore not disturb the measurements.

The model for the electron emission given in Eq. (12) assumes that the *ion beam is unpolarized* and that the *laser beam is linearly polarized*, and it can easily be shown that these requirements are fulfilled.

Stray electric fields, so called patch fields, cause problems in electron spectroscopy. Fortunately, these fields cause the electrons to change their paths stochastically, and the measured angular distribution is not changed in any particular direction. The effect appears as a statistical variation, and it should not be added to the systematic error. If the stray electric fields are very strong, the electrons are prevented from passing through the small holes in the graphite tube.

A *misaligned graphite tube* would change the measured angular distribution. The worst case, i.e. the worst misalignment which cannot be avoided, has been estimated. The change of the angular distribution has then been investigated with the same computer program as was used to compensate for the kinematic effect and the non-zero acceptance angle. This was performed by using an asymmetric integration interval, e.g. an horizontal acceptance angle between $+5°$ and $-7°$. The simulation showed that the ratio $I_{cm}(0°)/I_{cm}(90°)$ is changed by less than 0.01.

Finally, the effect of *reflection of electrons* from the surface of the graphite tube is treated. So far it has been assumed that each electron which strikes the surface of the graphite tube is grounded, but unfortunately this is not necessarily true. Electrons might be reflected, but it is very difficult to estimate the reflection coefficient of low energy electrons on a graphite surface [17]. In order to investigate the size of this effect the reflection coefficient is estimated to be less than 0.25, and it is assumed that the reflected electrons are scattered isotropically into a solid angle of 2π. The measured value of $I_{cm}(0°)/I_{cm}(90°)$ would then increase with less than 0.015.

6. Discussion

The main advantage with the apparatus described in this paper is that relatively weak processes can be studied with good signal levels. The neutral atom detector allows pulsed lasers to be used, which strongly increases the signal to background ratio. The angular distribution electron detector, which has an interaction path which is more than two orders of magnitude longer than all previous apparatuses, gives a signal which is significantly larger in comparison with other detectors.

Further, the apparatus may well be used to perform experiments with high optical resolution, and the reason for this is twofold: First, the general broadening mechanisms of the apparatus, like the beam divergence and velocity spread of the ions, are small. Secondly, as a consequence of the good signal levels, it is possible to perform experiments with very small statistical uncertainties.

In the future, a slow electron detector will be installed in the interaction region. This detector, initially developed at *JILA* [18], can be used to detect electrons with very small energy. It will be a complementary detector that can be installed without removing the present electron detector. Further, a new version of the angular distribution detector is under construction. The new version will detect electrons emitted in two perpendicular directions simultaneously. It will then be possible to measure the β parameter without rotating the polarization of the laser light. It will also be equipped with energy analyzers, making it possible to distinguish different photodetachment channels.

Acknowledgements

I am indebted to Jan-Åke Wiman for his skillful work in the mechanical machine shop and to Ove Eriksson for the technical assistance during the construction of the ion beam apparatus. Dr. Morgan Gustavsson is gratefully acknowledged for designing the data acquisition system. This work was financially supported by the Swedish Natural Science Research Council (NFR).

References

[1] W.H. Wing, G.A. Ruff, W.E. Lamb, Jr. and J.J. Spezeski, Phys. Rev. Lett. 36 (1976) 1488.
[2] M. Dufay, M. Carr'e, M.L. Gaillard, G. Meunier, H. Winter and A. Zgainski, Phys. Rev. Lett. 37 (1976) 1678.
[3] S.L. Kaufman, Optics Comm. 17 (1976) 309.
[4] D.M. Neumark, K.R. Lykke, T. Andersen and W.C. Lineberger, Phys. Rev. A 32 (1985) 1890.
[5] C.W. Walter, C.F. Hertzler, P. Devynck, G.P. Smith and J.R. Peterson, Nucl. Instr. and Meth. B 56/57 (1991) 216.
[6] M. Al-Za'al, H.C. Miller and J.W. Farley, Phys. Rev. A 33 (1986) 977.
[7] M.C. Baruch, T.F. Gallagher and D.J. Larson, Phys. Rev. Lett. 65 (1990) 1336.
[8] D. Berkovits, E. Boaretto, G. Hollos, W. Kutschera, R. Naaman, M. Paul and Z. Vager, Nucl. Instr. and Meth. B 52 (1990) 378.
[9] D.A. Dahl and J.E. Delmore, Simion PC/PS2, Idaho National Engineering Laboratory, EGG-CS-7233 Rev. 2 April (1988).
[10] H.D. Zeman, Rev. Sci. Instrum. 48 (1977) 1079.
[11] D Hanstorp, Meas. Sci. Tech. 3 (1992) 523.
[12] D. Hanstorp, C. Bengtsson and D.J. Larson, Phys. Rev. A 40 (1989) 670.
[13] N. Kashihira, E. Vietzke and G. Zellermann, Rev. Sci. Instrum. 48 (1977) 171.
[14] H. Hotop and W.C. Lineberger, J. Phys. Chem. Ref. Data 14 (1985) 731.
[15] D. Hanstorp and M. Gustafsson, J. Phys. B 25 (1992) 1773.
[16] E.P. Wigner, Phys. Rev. 73 (1948) 1002.
[17] N.L.S. Martin and A. von Engel, J. Phys. D 10 (1977) 863.
[18] R.D. Mead, K.R. Lykke, W.C. Lineberger, J. Marks and J.I. Brauman, J. Chem. Phys. 81 (1984) 4883.